PHYSICAL REVIEW B VOLUME 31, NUMBER 2 15 JANUARY 1985

Pulsed ion-beam melting of silicon

R. Fastow, Y. Maron,* and J. Mayer
Department of Materials Science and Engineering, Cornell University, Ithaca, New York 14853

(Received 10 April 1984)

Pulsed ion beams have been used to melt and regrow single-crystal silicon. By using the technique of transient conductivity, the effects of ion species and pulse duration have been determined. For heavier ions, with shorter pulses (70 ns), melt is initiated at lower energy densities. The regrowth velocity is also greater. For lighter ions (H^+) with longer pulses (140 ns), computer simulations show that the temperature gradient is uniform over the top 1.5 μm of silicon. Melt depths of up to 1.7 μm, and regrowth velocities as low as 1.2 m/s, are obtainable. For both types of pulses, the ion energies were distributed between 0 and 400 keV. The total energy density was varied between 0.76 and 2.0 J/cm^2.

INTRODUCTION

One possible application of pulsed ion beams is for surface modification of materials. Pulsed ion beams provide a unique alternative to laser or electron-beam annealing. An important parameter in pulsed ion-beam annealing is the ion species. By choosing a particular element, it is possible to control the penetration depth, and hence the resulting temperature profile in the substrate. For instance, protons deposit their energy nearly uniformly along their path (which for 300-keV protons into Si is 3 μm). 300-keV Ba ions, on the other hand, deposit most of their energy in the top 1000 Å of silicon. In certain applications, a small temperature gradient is desirable. Using protons, it is possible to anneal deeply implanted layers, or thick metallic contacts (5000 Å), without vaporizing the surface.[1] It has also been shown that metals can be heated uniformly to depths of 1 μm without destroying the surface.[2] An advantage of ion beams is that there is practically no reflection of energy. Thus the amount of energy deposited is independent of the phase material (the stopping cross section of silicon in the molten state is the same as that of silicon in the crystalline or amorphous state). More useful, however, may be the fact the SiO_2 absorbs roughly the same amount of energy as Si per unit of depth. The stopping power of SiO_2 for protons is 110 keV/μm, and the stopping power of Si is 95 keV/μm (at 200 keV). Another interest in pulsed ion beams is the simultaneous implantation and annealing of dopants.[3,4] Since the total fluency of ions is of the order of 5×10^{13} ions/cm^2, a relatively high doping density between 10^{15} and 10^{14} atoms/cm^3 can be achieved with a single pulse of As ions, for instance. At 300 keV, arsenic penetrates 1700 Å into silicon. This yields a doping density of 3×10^{18} atoms/cm^3 in the top 1700 Å.

EXPERIMENT

The purpose of this experiment was to observe the effects of ion species and pulse duration on pulsed ion-beam melted silicon. The melt depth and regrowth velocity as a function of time were measured by the technique of transient conductivity.[5] This technique has been used extensively in measuring the melt depth induced by laser irradiation of silicon.[6,7] It relies on the change in electrical

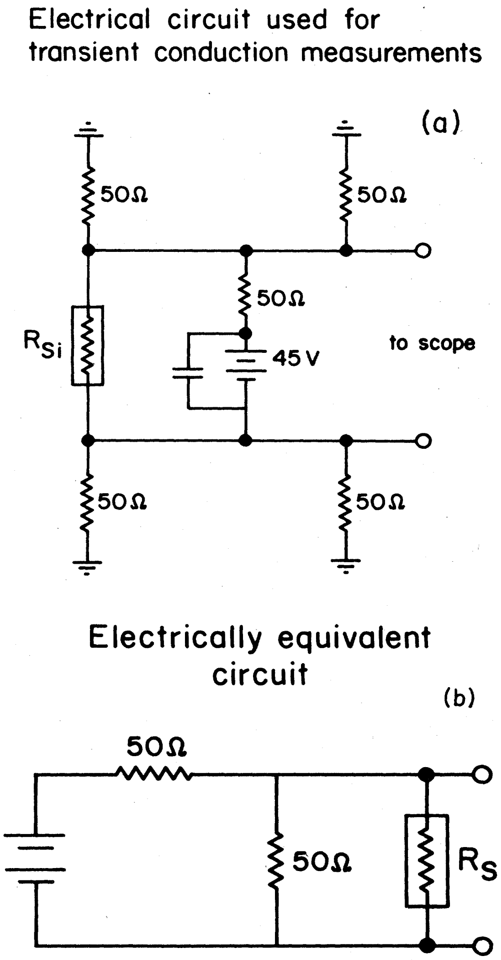

FIG. 1. Electrical circuit used for transient conduction measurements: (a) actual circuit; (b) electrically equivalent circuit.

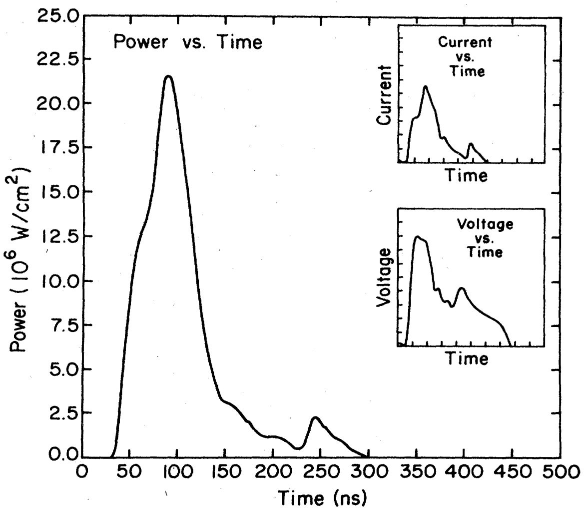

FIG. 3. Power vs time curve for the 70-ns ion pulse. The current and voltage scales for the insets are 10 amps/cm^2/div and 50 keV/div, respectively.

resistivity of silicon, upon melting. Crystalline silicon, for instance, has a resistivity of 2528 $\mu\Omega$ cm at its melting point of 1685 K. Doping with Au, which acts as a recombination center, reduces the carrier lifetime. The resistivity of molten silicon, however, decreases by a factor of 30 to 80 $\mu\Omega$ cm. Thus, by measuring the resistivity, it is straightforward to determine the thickness of the molten silicon layer. Figure 1 shows the actual and electrically equivalent circuit used for measuring the resistivity. The depth, in microns, can be determined by the following formula:

$$d=\frac{(0.064)(V)(l/w)}{45-2V}, \qquad (1)$$

where V is the voltage measured by the oscilloscope and l/w is the length/width ratio of the silicon sample.

The two 50-Ω resistors from the scope to the ground were used to prevent reflections in the coaxial cables. The 50-Ω resistors on either side of the silicon sample were used to minimize cable reflections, as well as to provide a pathway to dissipate excess charge. The problem of contact resistance with the sample was minimized by using a large length/width ratio. This was obtained by placing a thin slit, made of two glass cover slips, in front of the silicon sample. The length/width ratios were varied between 30 and 75; the length always being 1 cm. The oscilloscope, itself, was used in the differential amplifier mode. Figure 2 shows the oscilloscope trace of a 1.57-J/cm^2 pulse (70-ns pulse). The time scale was 200 ns/div, and the voltage scale was 2 V/div. The electrical noise during the first 400 ns was due to the ion flux and to electrical discharges in the diode. Faraday-cup measurements (Figs. 3 and 5) indicate that the incident ion current reached a maximum of 60 A/cm^2 for the 1.57-J/cm^2 pulse.

The incident energy density was varied by two methods. The first method was to place fine copper screens between the anode (source of ion beam) and the sample. This was necessary to reduce the beam intensity to usable levels. The second method was to change the sample to anode distance. Because the ion beam had a divergence of approximately 2°, this allowed significant variations in deposited energy. The total incident energy was measured calorimetrically. A low thermal mass chromel-alumel thermocouple was spot welded to the back of a thin nickel platelet. By measuring the temperature rise of the platelet, and knowing its thermal mass, the energy density of the pulse could be determined. The accuracy of this method is estimated at ±5% due to uncertainties in the thickness of the film, as well as film curvature, and beam inhomogeneities. The platelet and thermocouple were placed approximately 5 mm above the Si sample, so as to minimize problems with beam inhomogeneity.

Two different machines were used in order to change the beam parameters. The first machine (short pulse) produced an ion pulse of 70 ns in duration [full width at half-maximum (FWHM)]. Figure 4 shows the calculated power versus time curve, as well as the digitized voltage versus time and current versus time traces. The current was measured using a Faraday cup biased at -350 V. The voltage across the diode was measured using a resis-

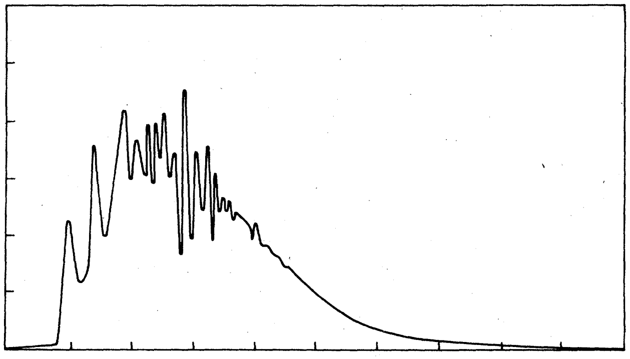

FIG. 2. Oscilloscope trace taken from transient conduction circuit. Vertical scale is 2 V/div, horizontal scale is 200 ns/div. This trace corresponds to a 1.6-J/cm^2, 70-ns ion pulse.

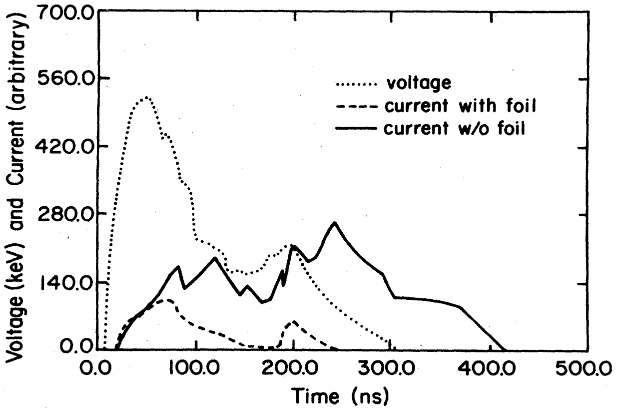

FIG. 4. Faraday-cup current vs time, with and without polyethylene stopping foil.

tive monitor, and was corrected for inductive effects. The composition of this beam was approximately 40% hydrogen, 60% carbon and aluminum (the three elements composing the diode). Traces of nitrogen and oxygen from the gas ambient may also have been present. The impurity concentration was determined by placing a 2-μm polyethylene foil in front of the Faraday cup during the pulse. The foil stopped the heavier ions, while letting through protons having an energy greater than 180 keV. Figure 4 shows the current traces with and without the polyethylene foil (for the same shot). The time of flight of the protons, a few tens of nanoseconds, was accounted for in the analysis. Integrating the current in both cases from 560 to 180 keV (corresponding to $t=0$ to $t=130$ ns) showed that the number of ions passing through the polyethylene foil was at most 40% of the total number of ions reaching the Faraday cup. Because of the longer time of flight of the heavy ions, a small percentage may not have been included in the integration. It was assumed that the same percentage of impurities was present in the second half of the pulse. No analysis was done on the reflected pulse ($t>130$ ns) because the trace was not reproducible. This behavior was attributed to ion-beam-induced plasmas in the Faraday cup.

The second machine (long pulse) produced an ion pulse of 140 ns in duration (FWHM). Figure 5 shows the calculated power versus time curve, as well as the digitized voltage versus time and current versus time traces. Experiments with polyethylene foil showed that the composition of the beam was 80% protons, 20% carbon and aluminum.[8] Thus, the two machines could be characterized in the following manner. The first machine produced a short (70-ns) pulse of mostly heavy ions. While the second machine produced a long (140-ns) pulse of mostly protons.

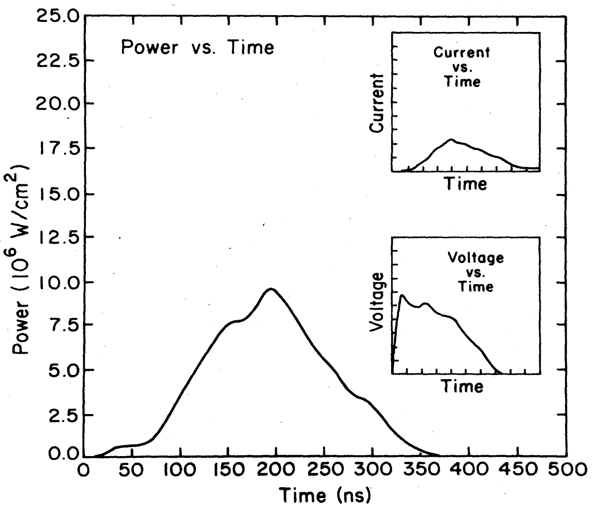

FIG. 5. Power vs time curve for the 140-ns ion pulse. The current and voltage scales for the insets are 10 amps/cm^2/div and 50 keV/div, respectively.

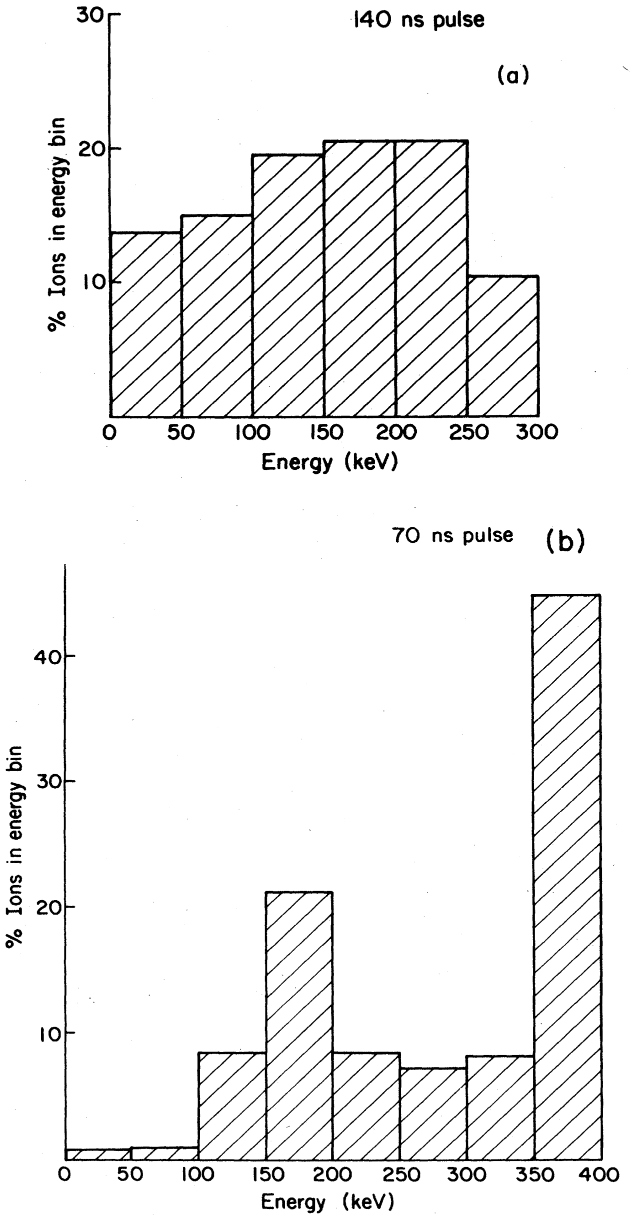

FIG. 6. Graph of ion-energy distribution for the 140-ns pulse: (a) 140-ns pulse; (b) 70-ns pulse.

Figure 6 shows the experimentally determined energy distribution for both the long and the short pulses. These distributions were determined by using the current and voltage data in Figs. 3 and 5. As can be seen, ions produced by the long pulse are fairly evenly distributed in energy between 0 and 300 keV. The average occurs at 150 keV. For the short pulse, however, the distribution is best described by two peaks. The one occurring at 350—400 keV corresponds to the primary pulse, and the one at 150—200 keV corresponds to the reflection in the transmission line. The reflection was caused by an impedance mismatch; 25 Ω for the diode and 10 Ω for the water line. Here, the average ion energy was 280 keV. Figure 7 shows deposited energy as a function of depth

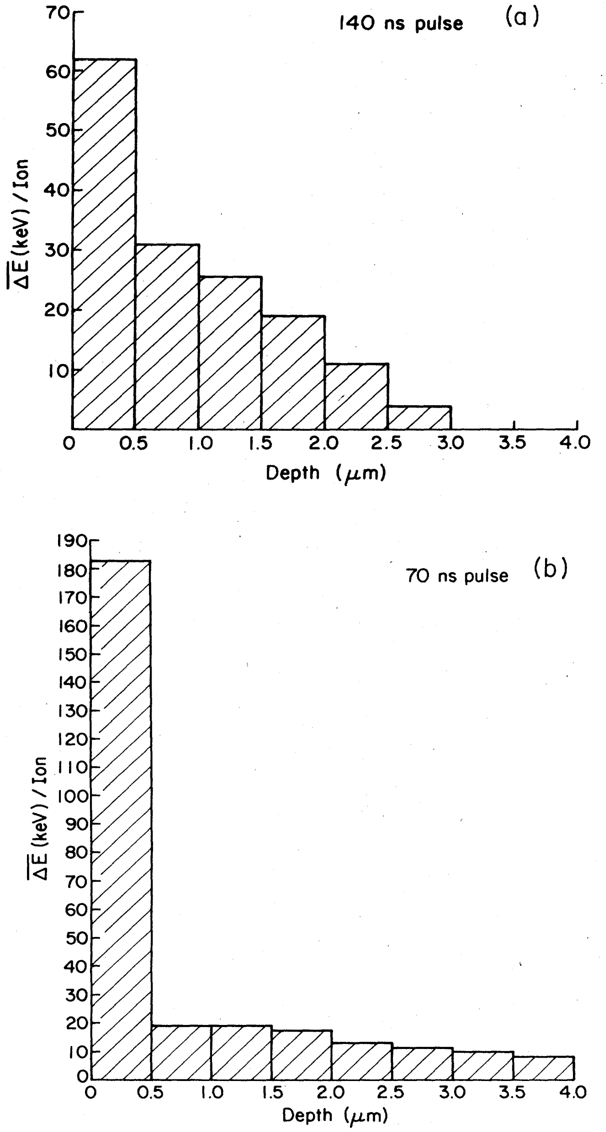

FIG. 7. Graph of ion-energy loss as a function of depth for (a) 140-ns pulse and (b) 70-ns pulse.

for the two machines. This graph was produced using the data in Fig. 6, as well as the known ranges of ions into silicon.[9]

RESULTS

The melt depth versus time curves for the 140-ns pulse (long pulse) are given in Fig. 8. Data for 2.0, 1.8, and 1.5 J/cm^2 pulses are shown. These curves were generated by applying formula 1 to the conductivity data, after the contribution due to photoconduction had been subtracted out. The increase in conductivity due to photoconduction was estimated by analyzing the conductivity versus time traces for low-energy pulses. It was found that these traces showed the same conductivity over the energy range of 0.7 to 0.95 J/cm^2; so they were taken as the photopeak. The photopeak lasted approximately 600 ns. The regrowth velocities were nearly the same for all incident energy densities (i.e., 1.2 m/s, at half the maximum melt depth). Figure 9 shows the melt depth versus time curves for the 70-ns pulse (short pulse). It is seen that for the highest incident energy density (2.0 J/cm^2) the maximum melt depth was only 1.0 μm; for 1.6 J/cm^2 the depth was 0.72 μm, for 1.0 J/cm^2, the depth was 0.45 μm, and for 0.8 J/cm^2, the depth was 0.2 μm. For the short pulse, the regrowth velocity decreased as the total beam energy increased. At 2.0 J/cm^2, the regrowth velocity was 1.1 m/s, whereas at 1.0 J/cm^2, the regrowth velocity was 2.4 m/s. In both cases (short and long pulse) these velocities were less than those obtained for laser-melted silicon. The measured regrowth velocity for silicon melted with a 30-ns ruby laser at 1 J/cm^2 was 2.8 m/s.[7]

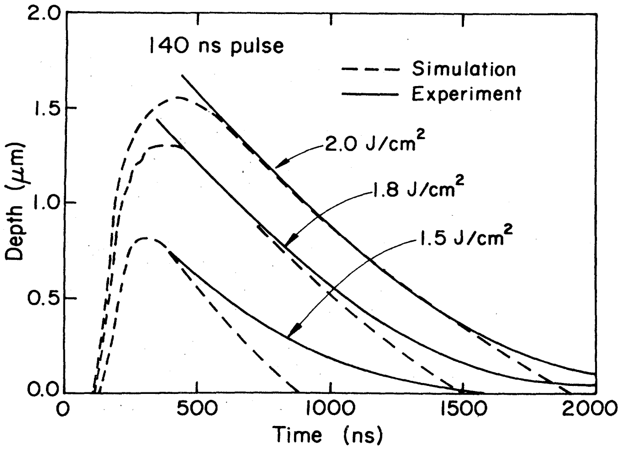

FIG. 8. Melt depth vs time curves for the 140-ns ion pulse.

Figure 10 shows a plot of the maximum melt depth as a function of total energy density for both pulses. In both cases the data points lie along straight lines. The slopes are 1.93 μm/J/cm^2 and 0.79 μm/J/cm^2, for the long and short pulses, respectively. The smaller value for the slope

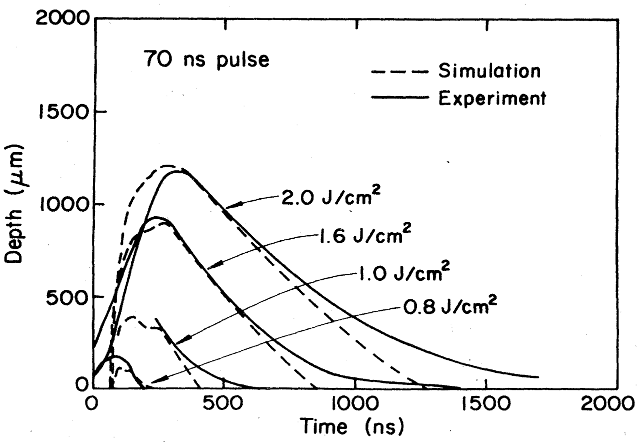

FIG. 9. Melt depth vs time curves for the 70-ns ion pulse.

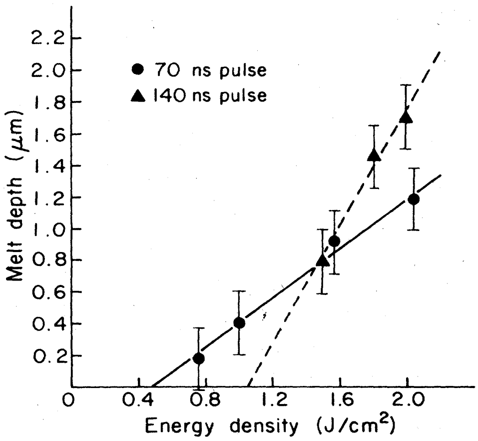

FIG. 10. Total melt depth vs incident energy density for the 70- and 140-ns pulses.

of the 70-ns pulse indicates that more energy is being lost to thermal conduction. Computer simulations (next section) show that the surface temperature gradient for this pulse is much larger than for the 140-ns pulse. The higher temperature of the surface is due to the high percentage of heavy ions. This high surface temperature can also be inferred from the lower value of the x-intercept.

SIMULATIONS

In Figs. 8–10, experimental melt depth versus time curves were compared to computer simulations. This section will describe the simulation. The computer program was divided into two parts. The first part modeled the ion pulse, and the second part calculated the heat flow in the substrate.

The ion pulse was simulated by using the time-dependent current and voltage traces as given in Figs. 3 and 5 (i.e., the long pulse was simulated by using the data in Fig. 5). From this, the energy deposited into the silicon, as a function of time and depth, was calculated using the energy-loss cross section of H, C, and Al, into silicon.[9] In the case of the carbon and aluminum ions, it was not known whether the ions were singly or doubly ionized, or the relative concentration of each element. Thus, an average penetration depth of 3000 Å was assumed. The total incident energy of the beam was varied by multiplying the current trace by an appropriate scaling constant.

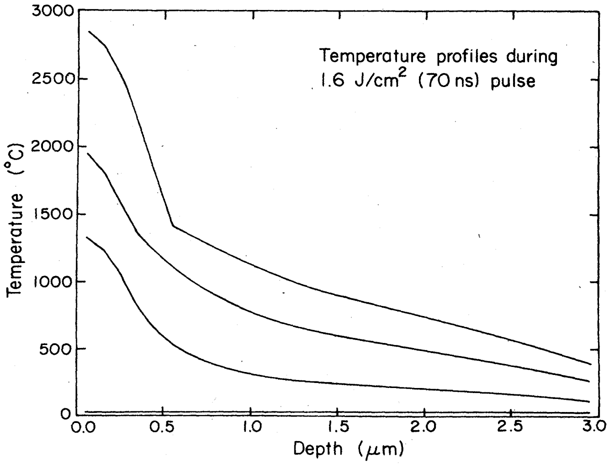

FIG. 11. Temperature profiles during a 1.6-J/cm², 70-ns ion pulse. Time increments are 20 ns.

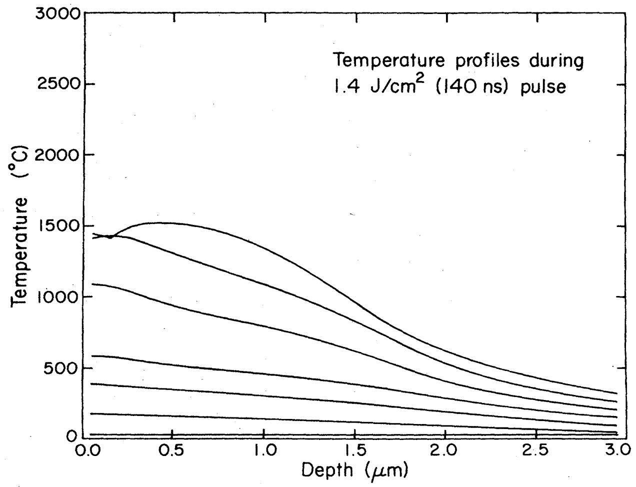

FIG. 12. Temperature profiles during a 1.4-J/cm², 140-ns ion pulse. Time increments are 20 ns.

The second part of the simulation concerned itself with the heat flow in the silicon. This part of the program was a numerical solution of the one-dimensional heat-flow equation. The temperature dependence of silicon's specific heat and thermal conductivity were included. It was assumed that melt began at the surface. This is obviously true for the 70-ns pulse, due to the high percentage of heavy ions. For the 140-ns pulse, Ge marker experiments show this also to be the case.[10] Figures 11 and 12 show computer simulations of the temperature profiles for both types of pulses. These simulations correspond to incident energy densities of 1.6 J/cm² for the short pulse, and 1.4 J/cm² for the long pulse. As can be seen in Fig. 11 (short pulse), steep temperature gradients are produced at the surface due to the heavy ions (1×10^7 K/cm). Whereas for the long pulse, relatively flat temperature gradients exist up to a depth of 1.5 μm. In fact a slight superheating of the interior is seen to occur due to the deep penetration depth of the protons. This flat temperature profile results in a smaller regrowth velocity.

DISCUSSION OF REGROWTH VELOCITY

The regrowth velocity, at times after the pulse, is related to the temperature gradient through the following formula:[6]

$$V=\frac{k}{\Delta H}\frac{\partial T}{\partial z}\bigg|_{\text{at interface}}, \qquad (2)$$

TABLE I. Regrowth velocity versus melt depth.

Melt Depth (Å)	$\frac{\partial T}{\partial z}$ (K/cm)	$\frac{k}{\Delta H}\frac{\partial T}{\partial z}$ (μ/sec)	V_{regrow} (m/sec) (computer generated)
3000	2.82×10^{6}	1.48	1.40
4500	3.21×10^{6}	1.68	1.60
7000	3.88×10^{6}	2.03	1.96

where k is the thermal conductivity, ΔH is the latent heat of fusion, and $\partial T/\partial z$ is the thermal gradient in the crystalline silicon. Equation (2) is a statement of the conservation of energy at the solid-liquid interface. The heat released during solidification, $v\Delta H$, must be conducted away by thermal diffusion, $k(\partial T/\partial z)$. According to this formula, as the temperature gradient becomes less, the regrowth velocity decreases.

There was excellent agreement between the regrowth velocity predicted by this formula, and the computer-calculated regrowth velocity. Equation (2) was applied to computer-calculated temperature profiles of pulsed ion-beam melted silicon. The values used for k and ΔH were 0.221 w/cm K and 4206 J/cm^3, respectively.[11,12] At different melt depths, the temperature profiles were different. Table I shows the calculated regrowth velocities at three different depths, produced by a 70-ns, 1.6-J/cm^2 ion pulse. These values were very close to the computer-generated regrowth velocities, which were calculated by Δ(depth of Si melt)/Δt (Table I).

SUMMARY

Pulsed ion-beam melting of silicon has been shown to be largely influenced by the ion species. For heavier ions, the penetration depth is less. This results in higher surface temperatures and steeper temperature gradients. For light ions (mostly H^+), the temperature is uniform over the top 1.5 μm of silicon. This results in lower regrowth velocities. In addition, a higher-energy density is needed to initiate melt. For both types of pulses, melt depths greater than 1 μm, and regrowth velocities as low as 1.2 m/s have been obtained.

ACKNOWLEDGMENTS

We wish to acknowledge Dave Hammer at the Cornell University Plasma Physics Lab for the use of the pulsed ion beam. This work was supported through the Cornell Materials Science Center by the National Science Foundation (L. Toth).

---

*Permanent address: Weizmann Institute, Tel Aviv, Israel.

[1] C. J. Palmstrom and R. Fastow, *Laser-Solid Interactions and Transient Thermal Processing of Materials* (Elsevier, New York, 1983).

[2] R. Fastow, J. Gyulai, M. Nastasi, and P. Zielinski, J. Mater. Sci. Lett. 3, 109 (1984).

[3] W. K. Chu, S. R. Mader, E. F. Gorey, J. E. E. Baglin, R. T. Hodgson, J. M. Neri, and D. A. Hammer, Nucl. Instrum. Methods **194**, 443 (1982).

[4] K. T. Hodgson, J. E. E. Baglin, R. Pal, J. M. Neri, and D. A. Hammer, Appl. Phys. Lett. **37**, 187 (1980).

[5] R. Fastow, J. Gyulai, and J. Mayer, *Laser-Solid Interactions and Transient Thermal Processing of Materials* (Elsevier, New York, 1983).

[6] M. Thompson, J. W. Mayer, A. G. Cullis, H. C. Weber, N. G. Chu, J. M. Poate, and D. C. Jacobson, Phys. Rev. Lett. **50**, 12 (1983).

[7] G. Galvin, M. Thompson, J. W. Mayer, P. S. Peercy, R. B. Hammond, and N. Paulter, Phys. Rev. B **27**, 1079 (1983).

[8] J. Neri, Ph.D. thesis, Cornell University, 1982.

[9] H. H. Anderson and J. F. Ziegler, *Hydrogen Stopping Power and Ranges in All Elements* (Pergamon, New York, 1977), Vol. 3.

[10] R. Fastow (unpublished).

[11] J. Phys. Chem. Ref. Data **1**, 394 (1972).

[12] *Progress in Semiconductors*, edited by A. F. Gibson (Heywood, London, 1960), Vol. 4, p. 259.